Available online at www.sciencedirect.com
ScienceDirect
Nuclear Instruments and Methods in Physics Research A 577 (2007) 231–237
NUCLEAR INSTRUMENTS & METHODS IN PHYSICS RESEARCH Section A
www.elsevier.com/locate/nima

Integrated simulation of an ion-driven warm dense matter experiment

Dale R. Welch[a,*], David V. Rose[a], Carsten Thoma[a], Adam B. Sefkow[b], Igor D. Kaganovich[b], Peter A. Seidl[c], Simon S. Yu[c], John J. Barnard[c], Prabir K. Roy[c]

[a]*Voss Scientific, 418 Washington SE, Albuquerque, NM 87108, USA*
[b]*Plasma Physics Laboratory, Princeton University, Princeton, NJ, USA*
[c]*Lawrence Berkeley National Laboratory, Berkeley, CA, USA*

Available online 22 February 2007

Abstract

Longitudinal compression factors in excess of 50 of a 300-keV, 20-mA K^+ ion beam have been demonstrated in the Neutralized Drift Compression Experiment (NDCX) in agreement with LSP particle-in-cell simulations using the experimental tilt voltage waveform. Here, pre-formed plasma provides beam neutralization for a 1–2-m drift length. To achieve simultaneous transverse and longitudinal compression, we must understand and account for the impact of the applied velocity tilt on the transverse phase space of the beam. Of equal importance to achieving warm dense matter and heavy ion fusion conditions, is quantifying the effect of beam plasma interactions, including stability and neutralization, on the beam transport throughout the drift section up to the target. Critical new issues relate to transverse focusing of the axially compressing ion beam in a high-field (3–15 T) solenoid that is filled with plasma. Integrated LSP simulations that include modeling of the diode, magnetic transport, induction bunching module, plasma neutralized transport, solenoidal focusing and beam target interaction, are assisting in the design of a near-term warm dense matter experiment. We discuss the simulation algorithms and present calculations of designs for such an experiment that will heat an aluminum target up to roughly 1-eV temperature.

PACS: 29.27-A; 52.65.Cc; 52.65.Rr

Keywords: Beam; Ion; Longitudinal compression; Plasma; Neutralization; Particle in cell

1. Introduction

Heavy ion fusion (HIF) and ion-driven warm dense matter (WDM) physics require the acceleration, compression, and transverse focusing of an intense ion beam. Neutralized drift compression (NDC) of an ion beam makes use of a temporal velocity tilt and neutralizing plasma to achieve short pulse lengths. In both HIF and WDM scenarios, a focusing force is applied to one or more ion beams outside the chamber. The ion beam energy must be transported to the target and deposited in a small spot before hydrodynamic disassembly. The physics of neutralized transport, in particular the feasibility of achieving a small transverse beam spot size in the presence of a neutralizing plasma, has been studied with simulations showing that small spots could be achieved with plasma neutralization [1]. A scaled experiment, the Neutralized Transport Experiment [2–5], subsequently demonstrated that an un-neutralized beam of several centimeter radius can be compressed transversely to ~1 mm radius when plasma neutralization is applied, in quantitative agreement with simulation [6,7].

Longitudinal compression in vacuum of space-charge-dominated beams has been studied extensively with theory and simulation [8–10]. The compression is initiated by imposing a linear head-to-tail velocity tilt to a drifting beam. Even under ideal conditions, longitudinal space charge limits the beam compression ratio R, the ratio of the initial-to-final current, to $R \leqslant 10$. An experiment with five-fold compression was reported [11]. In the presence of a perfectly neutralizing plasma, the compression is only limited by the accuracy of the applied velocity tilt and the ion longitudinal temperature [12]. Thus, this method has

*Corresponding author. Tel.: +1 505 255 4201; fax: +1 505 255 4294.
E-mail address: dalew@vosssci.com (D.R. Welch).

0168-9002/$ - see front matter © 2007 Elsevier B.V. All rights reserved.
doi:10.1016/j.nima.2007.02.057

demonstrated $R > 50$ on the Neutralized Drift Compression Experiment (NDCX) [13,14].

Here, we present an integrated numerical simulation with the capability to model ion acceleration, magnetic transport, NDC and focusing in a dense plasma as well as the interaction of the compressed beam with a target, which can be heated to temperatures in the highly coupled 0.1–1 eV WDM regime [15]. The various enabling algorithms available in the particle-in-cell (PIC) LSP simulation code include fast, implicit electromagnetic field solvers, energy-conserving particle advance, implicit particle-field advance and collision physics. With these algorithms, we can efficiently explore the tightly coupled physics of ion acceleration, compression and focusing of both near term planned experiments on the Solenoidal Transport Experiment (STX), shown in Fig. 1, and future possible WDM facilities using the High Current Experiment (HCX), both at the Lawrence Berkeley National Laboratory. The integrated simulations reveal the important interactions of the induction bunching module (IBM) geometry and solenoidal final focus with, and requirements on the neutralizing plasma.

The physical principles of NDC and final focusing are discussed in Section 2, and important LSP algorithms are outlined in Section. 3. Section 4 presents predictions for a combined longitudinal and transverse compression experiment on STX also and for an HCX-based WDM experiment, and conclusions are presented in Section 5.

2. Basic physics of NDC and final focus

We first examine the physics of an ion beam of energy E_i that is given a head-to-tail velocity tilt for longitudinal time-of-flight compression. The time-dependent velocity function at a particular plane that produces a perfect beam tilt for longitudinal compression at a downstream distance L is given by

$$v(t) = \frac{v(0)}{1 - (v(0)t/L)} \tag{1}$$

where $v(0)$ is the velocity of the pulse at $t = 0$. For the NDCX experiment with a 285-keV K^+ beam, the required

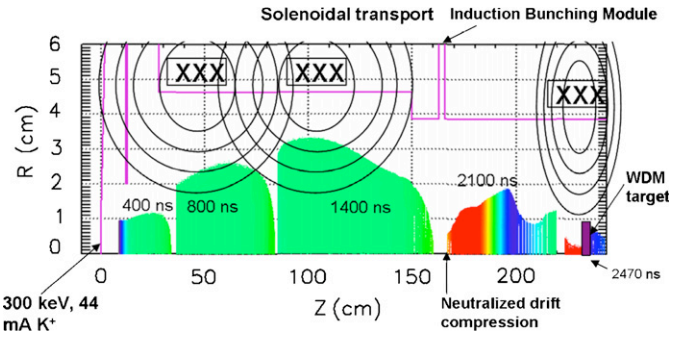

Fig. 1. Integrated simulation of the STX experiment beginning with the ion emitter at $z = 0$ and ending at a WDM target at $z = 235$ cm.

tilt voltage ramp in the linear regime (small tilt velocity-to-initial velocity ratio) is roughly $70/L$ kV/ns, or 0.7 kV/ns for a 1-m drift, and 0.35 kV/ns for a 2-m drift. In practice, the beam ion velocities will vary somewhat with a characteristic thermal longitudinal velocity $v_{||} = (kT_{||}/m_i)^{1/2}$ that limits the pulse length achievable to

$$t_{p\ \min} = \frac{L}{2c}\left[\frac{m_i c^2}{E_i}\right]\sqrt{\frac{T}{m_i c^2}} \tag{2}$$

where m_i is the beam mass and c is the speed of light. In the NDCX experiment, the voltage waveform required to produce the velocity profile in Eq. (1) was approximated with an IBM consisting of 14 independently driven magnetic cores.

A key issue concerning NDC involves the transverse focusing of the beam. Ultimately, the beam emittance limits the maximum tolerable focal length. The time-varying voltage at the accelerating gap imparts a time-dependent focal length to the beam. Simulations show that this effect limits the beam minimum radius to roughly 1 cm at the longitudinal focal position of the uncompressed beam. The gap across which the IBM voltage waveform is applied can be considered to be a bipotential lens, in which the radial component of the electric field is anti-symmetric about the center of the gap. In the paraxial approximation, the radial electric field E_r is proportional to r. Assuming a positive voltage difference $V(t)$ across the gap, the beam receives a net radial impulse upward on the upstream side of the gap and a net radial impulse downward on the downstream side of the gap. For a constant voltage, the slight change in the radius of particles as they traverse the gap results in an incomplete cancellation of the upward and downward radial forces and leads to a small net focusing effect. For NDCX, however, the ion beam moves relatively slowly and the gap voltage can change significantly during the ion transit time through the lens. So, the net radial forces upstream and downstream of the center of the gap do not cancel, since E_r is proportional to the time-dependent voltage, resulting in a transverse force imbalance on the beam ions. Using a simple thin-lens model, in which the radial forces are modeled by delta function impulses separated by the width of the gap, the time-dependent change in radial momentum of a nonrelativistic ion going through the gap can be approximated by

$$\Delta v_r \approx \frac{er}{2m_i v_z d}\left[\Delta V(t_0) - \Delta V(t_0 - d/v_z)\right] \approx \frac{e\dot{V}}{2m_i v_z^2} r \tag{3}$$

where v_z is the axial velocity of the ion and r is the radius of the ion upstream of the gap. The change of the axial velocity of the ion as it is accelerated across the gap is neglected, as is the change in radius. Therefore, a large and negative dV/dt, which is required for longitudinal focusing, also has a net transverse defocusing effect. The magnitude of this effect in the NDCX experiment can now be estimated assuming a 2-cm 285-keV beam and the previously calculated voltage ramps as 10 mrad for the 1-m

drift length and 5 mrad for the 2-m drift. Of course, the axial velocity is altered by the gap as well. The change in axial velocity is given by

$$\frac{\Delta v_z(t)}{v_z} = 1\sqrt{1 - \frac{2eV(t)}{m_i v_z^2}} \tag{4}$$

due to a change in tilt voltage $V(t)$. This gives a spread in axial velocity of about $\pm 10\%$ for a 285-keV beam and the real NDCX voltage waveform, resulting in a 2-mrad spread about a 20-mrad incoming angle for typical NDCX parameters. The total effect on the beam envelope is given by

$$a_0' = \frac{v_{r0} + \left(a_0 \Delta v_r(t)/(r)\right)}{v_{z0} + \Delta v_z(t)} \tag{5}$$

where a_0 is the disk edge radius at the gap. An envelope analysis, carried out for the same NDCX parameters as the LSP simulation, gives good agreement with the simulation.

Critical physics issues involve the neutralization of the compressing beam space charge by a plasma over many meters. From a simple 1D analysis, if stipulated that the beam impulse due to space charge (resulting in electric field E) over the neutralized drift, EL/v_z, must be less than the applied tilt, Δv, the neutralization fraction must satisfy

$$f > 1 - \frac{a_0^2}{2L^2 Z K(0)} \tag{6}$$

where $K(0)$ is the initial beam perveance defined by $K = 2I_b/I_A\beta^2$ with Alfven current $I_A = \beta\gamma m_i c^3/eZ$. Here, I_b, βc, γ, and Z are the beam current, velocity, relativistic Lorentz factor, and charge state, respectively. For typical HIF and WDM parameters, f must be >0.99. The presence of a high-density plasma ($n_p \gg n_b$) has been shown to provide this excellent charge neutralization in PIC simulations of HIF beam transport [1]. The plasma density condition requires increasingly higher plasma density as the beam compresses. A second obstacle, the electrostatic beam-plasma electron two-stream or Buneman instability, results in longitudinal emittance (or $v_{||}$) growth that could limit compression [16]. Recent work has shown that the instability typically saturates with negligible heating to a transverse focusing beam [17]. Highly spatially resolved 1D LSP simulations show that, for an axially compressing beam with NDCX parameters, the two-stream indeed saturates at a tolerable level that does not impact ideal compression in considered applications.

Finally, the addition of a strong final focus solenoid gives the ability to separate the focal length in the transverse plane from that of the longitudinal direction. This allows flexibility in allowing the beam to time-of-flight compression at a larger radius, thus reduces the requirements of plasma density and, with sufficient focusing strength, yields a shorter transverse focal length and tighter spot. However, there are two important caveats to this statement. First, the energy acceptance ΔE of the solenoid constrains the ratio of initial (a_0) to final (a_f) beam radius through

$$\frac{\Delta E}{E_i} = \frac{8a_f}{\pi a_0}. \tag{7}$$

Second, if the focal length of the beam with incoming velocity βc in the solenoid, $L_{sol} = \pi c\beta/2\Omega$ with $\Omega = B_z/2m_i$, becomes comparable to a_0, the pulse length is increased roughly by

$$\Delta t_{sol} = \frac{\sqrt{3}a_0^2}{12c\beta L_{sol}}. \tag{8}$$

3. Simulation tools for integrated modeling

3.1. PIC techniques

The LSP code possesses a wide range of field solution and particle advance options. In the integrated simulations, we make use of a fast, implicit electromagnetic field solver that is stable beyond the Courant limit [18], permitting time steps comparable to those used with electrostatic solvers in addition to increasing computational speed. In diode and accelerator regions, we use standard momentum-conserving PIC algorithms for the beam ions. Volumetric plasma electrons can be described with a robust energy-conserving particle advance model, including particle collisions, using kinetic equations. Inertial fluid equations are used to advance the Al target electrons and ions. Here, the implicit particle-advance algorithm is useful where the details of electron plasma oscillations can be ignored. The energy-conserving algorithm does not require resolution of the Debye length and avoids grid heating even when the time steps are small, $\omega_p \Delta t < 1$, where, ω_p is the plasma frequency and Δt is the simulation time step. Electron collisionality in the Al target is modeled in Monte Carlo fashion with energy, temperature, and charge state-dependent cross-sections, as described by the Lee–More model [19] with Desjarlais corrections [20]. and the ion charge state is calculated with a Thomas–Fermi equation-of-state involving pressure ionization corrections. These algorithms are described in detail elsewhere [21].

For very large integrated simulations, we use a faster, but approximate, inertialess plasma algorithm to describe the plasma current response with Ohm's law: $J = \sigma(E + v \times B)$, where the conductivity $\sigma = e^2 n_e/m_e v_m$ and v_m is the plasma electron momentum transfer frequency assuming Spitzer collisions.

3.2. Benchmark with NDCX data

We now make detailed comparisons between the measured and simulated NDCX ion transport with and without plasma neutralization in the 1- and 2-m drift sections. In this experimental series, a phototube diagnostic [13,22] is used to measure beam pulse compression with and without neutralization. The data are compared with LSP simulations using the measured IBM waveform for the

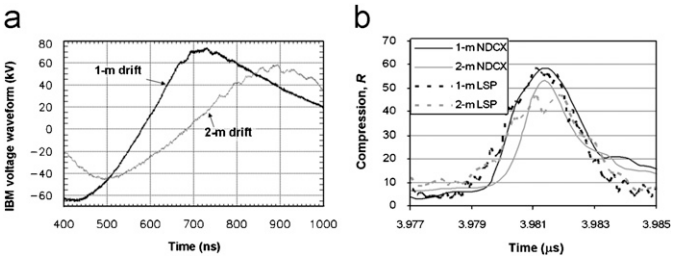

Fig. 2. In (a) the tilt waveforms used in the 1 and 2-m experiments are plotted corresponding to 21 and 15.75 kV. Comparison of R from the 1- and 2-m NDCX data and LSP simulation assuming 0.2-eV beam temperature are shown in (b). The data and simulations were time shifted to that of the 1-m data.

1- and 2-m drift experiments shown in Fig. 2a. The K^+ ions are injected at $z=-27$ cm into a 3.8-cm radius tube with a 260–320-keV mean energy, 1.9-cm outer radius, and a 0.21-eV source temperature that is isotropic in the transverse and longitudinal directions. The incoming focusing angle is 7.5 or 13.5 mrad for the 2 and 1-m drift lengths, respectively. The waveform is injected (after 200 ns) into a radial waveguide, with gap extending from $z=-22$–19 cm, giving enough time for 160 ns of beam pulse to precede the compressed portion of the beam. A uniform $10^{10}\,\mathrm{cm}^{-3}$ plasma density is modeled at $t=0$ for $z>-5$ cm. An electrostatic trap centered at $z=-12$ cm prevents plasma electrons from moving upstream on the time scale of the beam pulse. Further details of the experiment can be found in Refs. [13,14].

As discussed in Section 2, the ultimate limitation on beam axial compression is the beam longitudinal temperature. The measured ion source temperature of 0.21 eV is assumed in the simulations. In Fig. 2b, we compare the best data and simulation R values for the 1- and 2-m drift lengths. The curves are time shifted to the 1-m data to line up the maxima. We see that the pulse widths are quite small with a 3- and 2.5-ns full-width at half-maximum (FWHM) for the 1- and 2-m data, respectively. The similar widths indicate that the beam temperature must indeed be small compared with the tilt errors. The simulations give slightly wider pulses, roughly 3 ns for both lengths. If we assume that the minimum pulse width is dominated by the source temperature in the 2-m drift experiment, we deduce the upper bound for the source temperature as 1 eV. However, considering the simulations use 0.21 eV and give roughly the same R values and pulse widths, the beam temperature is likely cooler and closer to the simulation value.

4. Integrated simulation of NDC and final focus

In this section, we present two examples of the integrated simulation models that include the near term 300-keV STX and 1.6-MeV HCX designs. Because of the relative simplicity of the STX design with solenoidal transport, we include the full beam acceleration, transport and focusing. Because of the inherently 3D nature of quadrupole transport of the HCX design, we begin those simulations just upstream of the IBM.

4.1. STX experiment

Because the STX accelerator makes use of solenoidal transport, demonstrating the integrated simulation capability in 2D due to its inherent azimuthal symmetry is an ideal problem. A feasible experimental setup that includes the injection and acceleration of the K^+ beam to 300 keV and 44-mA, two 2.446 T, 40-cm solenoids for transport and initial focus, the IBM at $z=172$ cm, and a NDC section with a 15-T, 13-cm final focus solenoid at $z=231$ cm shown in Fig. 1. The beam ions at different times are plotted with energy indicated by color (blue to red indicates 200–400 keV energy particles). The velocity tilt is evident after the beam has passed through the IBM. The incoming angle of the beam is increased to adjust for the radial defocusing (Eq. (3)). This fully integrated electromagnetic simulation made use of an Ohm's model for the plasma current response, which assumes a 3-eV, 3×10^{12}-cm^{-3} density plasma. The injected IBM waveform is ideal for a 200-ns, 300-keV beam pulse with an axial focus at $z=235$ cm.

The calculated beam just upstream of the IBM has $T_{||}\sim0.01$ eV with a 0.08-π-mm-mrad normalized emittance ($T_{\perp}\sim0.2$ eV). The very cold axial temperature is a result of the conservation of longitudinal emittance in the diode (with applied voltage V) which reduces the beam temperature from that of the source T_s as described by $kT_{||}=(kT_s)^2/(2\,\mathrm{eV})$ [23]. Given adequate temporal resolution, the PIC results approach this formula. Such a cold beam, if given a perfect tilt and focusing angle, would yield a 100-ps pulse with $R=2000$. Shown in Fig. 3, the STX beam shows good $R=45$, since only a fraction of such an extreme compression is possible. Although the effect of the strong solenoidal field adds roughly 1 ns of pulse duration to the beam, as described in Section 2, R is reduced mainly by the finite gap distance which smears the ideal voltage pulse. The beam transit time across the gap is roughly 25 ns, which is too large for the 200-ns IBM pulse, giving roughly 20% of the pulse a nonideal (nonlinear) tilt. In addition, the beam emittance should ideally produce a

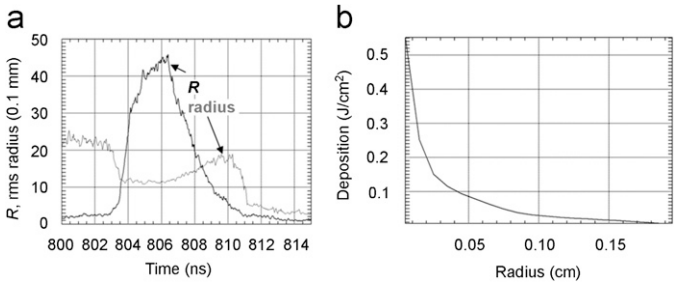

Fig. 3. The longitudinal compression and rms radius at $z=235$ cm are plotted in (a) for the integrated STX simulation. In (b), the time-integrated energy deposition at the same plane is shown.

0.35-mm rms radius spot at $z = 235$ cm. We calculate an rms radius that is a factor of 3 larger. Once again, this degradation is due to the IBM gap geometry causing an axial sweep in the beam focus described in Section 2. The time-integrated energy deposition also shown in Fig. 3 calculates a maximum of 0.55 J/cm^2 which, ignoring hydrodynamic expansion produces a roughly 0.19-eV peak temperature in an Al target (assuming 3 eV/eV-atom specific heat).

4.2. HCX-based WDM experiment

We can mitigate many of the IBM gap related problems observed in the STX simulations by increasing the beam energy. In contrast, the HCX accelerator is capable of producing a 1.6-MeV, 0.36-A K^+ beam with longitudinal temperature on the order of 1.67 eV. To obtain a comparison with the lower energy STX, we begin our simulations just upstream of the IBM gap and use the same gap geometry, 15 T focusing solenoid, and 1.9 cm beam edge radius as the STX case. For convenience, we assume that the transverse temperature is also 1.67 eV, which gives a 0.25-π-mm-mrad emittance. The IBM pulse length is reduced to 50 ns with an ideal 200-kV voltage waveform, giving an axial focal length of 220 cm. This short IBM pulse is not compensated by the faster beam and will limit R, as in STX. The fractional variation in tilted beam energy in this case will be 0.125, which should allow for a better focus in the 15-T final focus solenoid. The HCX final focus schematic with snapshots of the beam is seen in Fig. 4.

Shown in Fig. 5, the beam reaches 8 A ($R = 24$), with a 0.35-mm-rms final spot radius. Once again, because of the transit time of the beam across the gap, R is reduced from the ideal case (88). However the rms radius is only 40% larger than that allowed by the emittance. Because of the larger initial current and smaller radius, we see the energy fluence increases to 6.7 J/cm^2 which yields roughly a 0.6-eV temperature in Al.

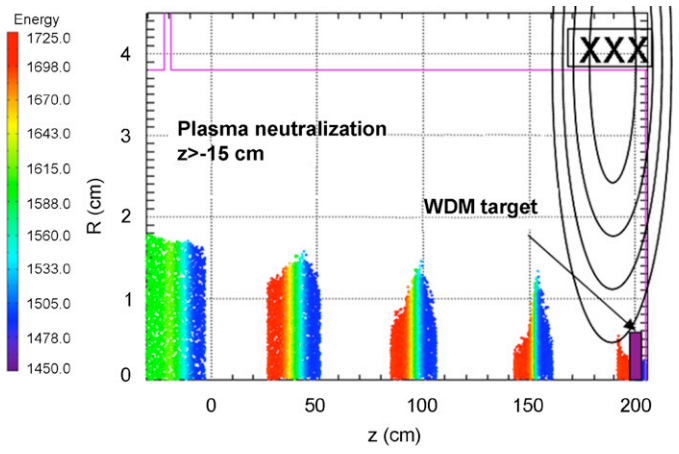

Fig. 4. The HCX final focus simulation geometry and beam snapshots at 100, 300, 500, 700, and 860 ns are shown.

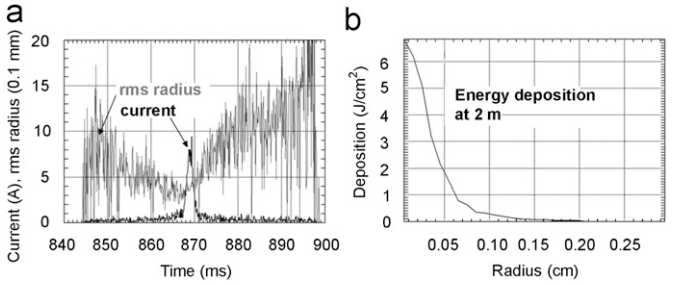

Fig. 5. In (a) the compression and rms radius of the HCX beam are shown and (b) the energy deposition at the $z = 200$ cm plane.

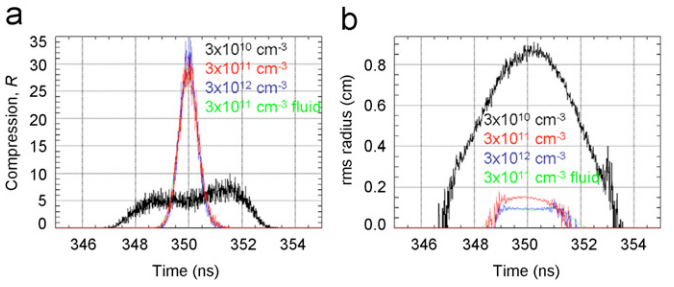

Fig. 6. The (a) compression and (b) rms radius calculated from the HCX kinetic and fluid plasma simulations are shown at the 95-cm plasma. The beam enters the simualtion with a 2-cm radius, 0.72-A current. A 5-T, 20-cm solenoid is centered at 50 cm.

4.3. Kinetic plasma simulations

We have used an idealized model for the plasma to this point in order to calculate the neutralization in the simulations. We now more accurately assess the plasma neutralization in a series of kinetic plasma simulations. We make two simplifications to allow for faster computation. First we start the simulations with the HCX beam example already compressed by 2 (25-ns pulse, 0.72-A current and ideal tilt already applied), which reduces the simulation length to 100 cm. The beam temperature is accordingly increased by 4. Secondly, the peak solenoidal fields are reduced to 5 T which allows a speed-up of the simulations because the required temporal resolution of the electron cyclotron frequency is reduced by a factor of 3. The 20-cm solenoid is placed at $z = 50$ cm and the focus is actually at $z = 95$ cm where the solenoidal field is only 250 G. The change allows the WDM target to reside outside the strong fields. Three cases of uniform kinetic plasma are initialized, corresponding to densities of 3×10^{10}, 3×10^{11}, and 3×10^{12} cm^{-3}. We also ran a 3×10^{11}-cm^{-3} plasma case with the inertialess fluid model for comparison. The results from the four simulations are shown in Fig. 6. We see R is best in the kinetic simulations with the 3×10^{12} cm^{-3} plasma case; the rms radius is near ideal at 1 mm (3 × larger due to the smaller solenoidal focusing field). The 3×10^{11}-cm^{-3} kinetic simulation gives the same compression but increased radius at focus. The fluid model with 3×10^{11} cm^{-3} density compares well with the kinetic

simulation at highest density. Thus, the fluid model overestimates neutralization particularly as the beam density approaches that of the plasma.

4.4. Simulation of WDM target interaction

In an actual experiment to access WDM conditions, it is desirable for the ion beam to strike the target at its peak compressed density. We would also like the beam energy to be deposited before significant hydrodynamic expansion of the target (isochoric heating). If the target is too thin or the ion range is too short, the target can lose its solid integrity and expand before the entire beam energy is deposited. Because of this effect, for the HCX beam energy (the energy loss rate for Al is 6.97 MeV cm^2/mg) we would prefer to use a lower density foam-like material. In our example, we assume a 1/10 density Al target of 4.8-μm thickness. The 1.6-MeV K^+ ions then lose half of their energy before leaving the target. Several issues can be studied in this final stage of the "integrated simulation", including the hydrodynamic expansion of the target, beam self-field effects, and target charging.

In the simulation, we assume the ion beam current and radial profile to be as shown in Fig. 5a. The assumption of a constant radial profile is only an approximation, in that the beam rms radius grows by 20% during the peak beam compression. Since we must begin the simulation near the beginning of the compressed beam pulse, the peak beam current occurs at 2 ns into the target interaction simulation. The 1/10 density, 1-mm radius Al target is also surrounded by a 3-eV, 3×10^{12} cm^{-3} Al^+ plasma (such as that from a MEVVA plasma source for neutralization). The simulation space extends an additional 1 mm on either side of the target and 2 mm in radius. The numerical grid is axially fine in the region of the target (0.2 μm), but increases significantly away from the target. The beam interaction with the target is somewhat simplistic. We use the 6.97 MeV-cm^2/mg constant energy loss rate and assume that beam strips up to a +3 equilibrium value for 1.6 MeV with constant 10^{-16} cm^2 stripping cross-section in Al. Thus, two electrons are left behind in the target as each K^{3+} ion leaves the target, giving the possibility of target charging.

The peak temperature is reached after 3 ns, yielding a 0.83-eV temperature near the center of the target. In Fig. 7, we see that the highest heating has occurred within a 0.15-mm radius. At this point in time, the target density has decreased 20% from its initial density due to the hydrodynamic response. Because of this expansion, the target temperature does not heat further after 3 ns despite continuing beam energy deposition (<10% of total). There is also a cooler 10^{17}-cm^{-3} density foot that extends 20 μm from the target on both sides which could complicate measurements in the highest-temperature region. The impact of the beam self fields is minimal on the beam–target interaction. The peak electric fields, which include both inductive fields from the growth of the roughly 5-A net current (sum of the beam and plasma currents) and electrostatic fields due to the beam non-neutralization and target charging, are not more than 10 kV/cm. The target charges during the beam pulse to roughly −20 V yielding a well defined potential sheath at the target edges with negligible electric fields in the dense region of the target. Thus, for these conditions, the field impact when compared with the collisional energy loss is negligible and the interaction is essentially classical.

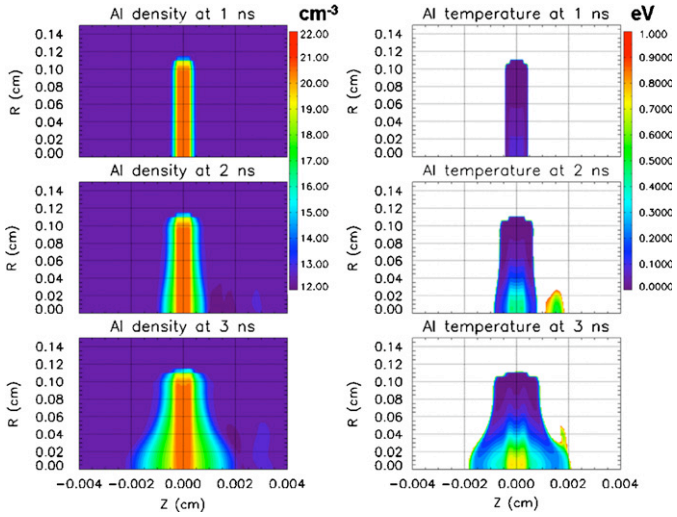

Fig. 7. The Al target density (left column) and temperature (right column) are plotted at 1, 2 and 3 ns for the HCX beam interaction with a 4.8-μm thick, 1/10 density Al target.

5. Conclusions

We have demonstrated an integrated simulation capability to study the longitudinal and transverse focusing of ion beams for WDM applications, as well as certain realistic effects which reduce the amount of total compression compared to ideal expectations. With plasma to provide neutralization, we have observed good longitudinal compression in excess of 50 in both experiment and LSP simulation. The compression requires adequate control of both the beam longitudinal temperature and tilt waveform. The plasma permits a transversely focusing beam to achieve smaller spots as the axial compression progresses without significant beam degradation due to beam-plasma instability. The compression ratio observed for a 2-m drift is consistent with a <1-eV longitudinal beam temperature, indicating little heating due to transport or beam-plasma interaction.

The transverse focusing of the compressed pulse is complicated by the time dependence of the voltage. Because the radial defocusing from the tilt gap depends largely on the applied rate of voltage increase, we have found that the bulk of the defocusing can be compensated for upstream by applying a larger angle. Integrated simulations of the upcoming STX experiment predicts that

simultaneous focusing of the axial and transverse planes is achievable. Simulations of HCX transport and focusing coupled to an Al foam target predict near-isochoric heating to 0.83 eV.

Acknowledgments

This research was supported by the US Department of Energy under Contract no. DE-AC02-05CH11231 with the Lawrence Berkeley National Laboratory, Contract no. DE-AC02-76CH03073 with Princeton Plasma Physics Laboratory, and Contract no. DE-W-7405-Eng-48 with Lawrence Livermore National Laboratory for Heavy Ion Fusion Science-Virtual National Laboratory.

References

[1] D.R. Welch, D.V. Rose, B.V. Oliver, R.E. Clark, Nucl. Instr. and Meth. A 464 (2001) 134.
[2] S. S. Yu, et al., in: J. Chew (Ed.), Proceedings of the 2003 Particle Accelerator Conference, Portland, Oregon, 2003, IEEE, USA, 2003, p. 98.
[3] E. Henestroza, S. Eylon, P.K. Roy, et al., Phys. Rev. ST Accel. Beams 7 (2004) 083501.
[4] P.K. Roy, S.S. Yu, S. Eylon, et al., Phys. Plasmas 11 (5) (2004) 2890.
[5] B.G. Logan, et al., Nucl. Fusion 45 (2005) 131.
[6] C. Thoma, D.R. Welch, S.S. Yu, E. Henestroza, P.K. Roy, S. Eylon, E.P. Gilson, Phys. Plasmas 12 (4) (2005) 043102.
[7] P.K. Roy, S.S. Yu, S. Eylon, et al., Nucl. Instr. and Meth. A 544 (2005) 225.
[8] D.D.-M. Ho, et al., Particle Accelerators 35 (1991) 15.
[9] H. Qin, R.C. Davidson, J.J. Barnard, E.P. Lee, Phys. Rev. ST Accel. Beams 7 (2004) 104201.
[10] W.M. Sharp, J.J. Barnard, D.P. Grote, et al., Nucl. Instr. and Meth. A 544 (2005) 398.
[11] W.M. Fawley, T. Garvey, S. Eylon, E. Henestroza, A. Faltens, T. Fessenden, K. Hahn, L. Smith, D. Grote, Phys. Plasmas 4 (3) (1997) 880.
[12] D.R. Welch, D.V. Rose, T.C. Genoni, S.S. Yu, J.J. Barnard, Nucl. Instr. and Meth. A 544 (2005) 236.
[13] P.K. Roy, S.S. Yu, E. Henestroza, et al., Phys. Rev. Lett. 95 (2005) 234801.
[14] A.B. Sefkow, R.C. Davidson, P.C. Efthimion, et al., Phys. Rev. ST Accel. Beams 9 (2006) 052801.
[15] S. Ichimaru, Rev. Mod. Phys. 54 (1982) 1017.
[16] E. Startsev, R.C. Davidson, Phys. Plasmas 13 (2006) 062108.
[17] D.V. Rose, T.C. Genoni, D.R. Welch, E.P. Lee, Nucl. Instr. and Meth. A 544 (2005) 389;
T.C. Genoni, D.V. Rose, D.R. Welch, E.P. Lee, Phys. Plasmas 11 (2004) L73.
[18] F. Zheng, Z. Chen, J. Zhang, IEEE Trans. Microwave Theory Tech. 48 (2000) 1550;
F. Zheng, Z. Chen, IEEE Trans. Microwave Theory Tech. 49 (2001) 1006.
[19] Y.T. Lee, R.M. More, Phys. Fluids 27 (1984) 1273;
R.M. More, et al., Phys. Fluids 31 (1988) 3059.
[20] M.P. Desjarlais, Contrib. Plasma Phys. 41 (2001) 267.
[21] D.R. Welch, D.V. Rose, R.E. Clark, T.C. Genoni, T.P. Hughes, Comp. Phys. Comm. 164 (2004) 183;
D.R. Welch, D.V. Rose, M.E. Cuneo, R.B. Campbell, T.A. Mehlhorn, Phys. Plasmas 13 (2006) 063105.
[22] F.M. Bieniosek, S. Eylon, A. Falens, et al., Nucl. Instr. and Meth. A 544 (2005) 268.
[23] See M. Reiser, Theory and Design of Charged Particle Beams, Wiley, New York, 1994.